Effect of the heat treatment on the microstructure, magnetism and magnetocaloric effect in Fe-rich (Mn,Fe)$_y$(P,Si) melt-spun ribbons

Kiecana, A.; Kwakernaak, C.; van Dijk, N. H.; Brück, E.

Important note
To cite this publication, please use the final published version (if applicable).
Please check the document version above.

Effect of the heat treatment on the microstructure, magnetism and magnetocaloric effect in Fe-rich $(Mn,Fe)_y(P,Si)$ melt-spun ribbons

A. Kiecana [a],[*], C. Kwakernaak [b], N.H. van Dijk [a], E. Brück [a]

[a] *Fundamental Aspects of Materials and Energy Group, Department of Radiation Science and Technology, Faculty of Applied Sciences, Delft University of Technology, Mekelweg 15, 2629JB Delft, the Netherlands*
[b] *Department of Materials Science and Engineering, Delft University of Technology, Mekelweg 2, 2628 CD Delft, the Netherlands*

A R T I C L E I N F O

A B S T R A C T

The effect of the heat treatment on the magnetism, magnetocaloric effect and microstructure formation has been systematically studied in Fe-rich $(Mn,Fe)_y(P,Si)$ melt-spun ribbons ($1.80 \leq y \leq 2.00$). XRD, SEM and EDS measurements demonstrate that a metal deficiency prompts the stable $(Mn,Fe)Si$ phase, whereas in the metal-rich region the $(Mn,Fe)_3Si$ phase is formed. It is found that the annealing temperature influences the composition and lattice parameters of the $(Mn,Fe)_y(P,Si)$ alloys, which greatly affects the Curie temperature (T_C). For the optimal metal/non-metal ratio y the magnetic entropy change ($|\Delta S_m|$) is found to increase from 5.5 to 15.0 $Jkg^{-1}K^{-1}$ in a magnetic field change of 2 T by varying the annealing temperature from 1313 to 1433 K, indicating an enhancement of the first-order magnetic transition (FOMT). The presented results reveal that the secondary phase and magnetic properties in the $(Mn,Fe)_y(P,Si)$ system can be tuned by varying the annealing temperature and by adjusting the metal/non-metal ratio y.

1. Introduction

The magnetocaloric effect (MCE), discovered in 1917 by Weiss and Picard [1], is a phenomenon that corresponds to a change of temperature caused by the exposure of a material to an externally applied magnetic field. Although the giant magnetocaloric effect (GMCE) was first observed in Fe-Rh alloy by Annaorazov and co-workers [2], the interest in the application of magnetocaloric materials (MCM) in magnetic cooling started from the discovery of the GMCE in $Gd_5Ge_2Si_2$ by Pecharsky and Gschneidner [3]. This breakthrough research was followed by another milestone: the demonstration of near room-temperature magnetic-refrigeration prototype by Zimm and co-workers [4]. In comparison to traditional cooling technologies, magnetic cooling provides a significantly higher efficiency, and the environmental impact is reduced due to the elimination of hazardous, toxic and ozone-depleting refrigerants [5]. Materials exhibiting a first-order magnetic transition (FOMT) attract special attention due to the presence of a GMCE, usually associated with it [6–8]. Until now, many promising families of MCMs for the near-room temperature refrigeration have been studied intensively, e.g.: Fe-Rh [9–11], $Gd_5(Si,Ge)_4$ [3,12,13], $LaFe_{13-x}Si$ [14–16],

$(Mn,Fe)_2(P,X)$, (X = As, Ge, Si) and its doped compounds [8,17–20] and Heusler alloys [21,22].

Among the mentioned magnetocaloric materials, the $(Mn,Fe)_2(P,Si)$ family of compounds that exhibit a large MCE in low magnetic fields near room temperature have drawn considerable attention. The Fe-rich region of the $(Mn,Fe)_2(P,Si)$ system is especially of interest due to its large magnetic moment and low costs of starting materials [20]. It has recently been reported that in this family of compounds, the metal/non-metal ratio (M/NM) has a significant impact on the final performance of the material [6,23]. Additionally, the magnetocaloric response of the $(Mn,Fe)_2(P,Si)$ system appears to be highly sensitive to the synthesis route, particularly to the heat treatment conditions [24–26]. In order to reduce the annealing time and avoid oxides impurities, all samples in this study were prepared by melt spinning. Notwithstanding extensive studies on the impact of optimization and annealing, the effect of the heat treatment for different M/NM ratios on the final performance of the material and formation of impurity phases was not investigated yet. Therefore, the main objective of this work is to study the effect of the metal content and the heat treatment on the magnetic properties, microstructure and impurity phase formation in Fe-rich $(Mn,Fe)_y(P,Si)$ melt-spun ribbons.

* Corresponding author.
E-mail address: A.Kiecana@tudelft.nl (A. Kiecana).

2. Experimental methods

$Mn_{0.68}Fe_{y-0.68}P_{0.66}Si_{0.34}$ (y = 2.00, 1.95, 1.90, 1.85, 1.80) compounds were prepared by melt spinning and subsequent annealing. These compounds will for simplicity in the following be denoted as $(Mn,Fe)_y(P,Si)$, where y then also corresponds to the M/NM ratio in the $(Mn,Fe)_y(P,Si)$ system. Appropriate amounts of the starting materials (powders): Mn (99.9 %; Alfa Aesar), Si (99.7 %; American elements), MnP (99.8 %; BASF), Fe_2P (99.9 %; BASF), were weighed, mixed and ball milled together for 1 h at 350 rpm. The purity of starting materials was determined on a metals basis. Powders were pressed into pellets and put into a quartz tube with a nozzle at the bottom. The as-spun ribbons were obtained by melting and ejection of the alloy through the nozzle on a rotating copper wheel. Prepared ribbons were placed in quartz tubes and sealed under 200 mbar Ar atmosphere before utilizing various heat treatments. All samples were annealed for 2 h at different temperatures. In order to minimize the formation of the metal-rich $(Mn,Fe)_3Si$ impurity phase, the oven was set to a target temperature before inserting the samples. In the first part of this study, we focussed on the optimization of the M/NM ratio. Therefore, the as-spun ribbons were annealed at 1373 K, which was found to be the optimal annealing temperature in an earlier report by Thang and co-workers [26]. In the second part of this study, we investigate the effect of the heat treatment by comparing samples from the first part of this study with melt-spun ribbons annealed at 1313 and 1433 K.

X-ray diffraction patterns were collected using a PANalytical X-pert Pro diffractometer with Cu-K$_\alpha$ radiation. Structural parameters and phase fractions were obtained by Rietveld refinement using the Fullprof program [27]. Magnetic measurements were conducted using superconducting quantum interference devices (SQUID) MPMS-XL and MPMS-5S magnetometers in the reciprocating sample option (RSO) mode, in the temperature range of 5–370 K with a constant sweep rate of 2 K/min. Differential scanning calorimetry (DSC) measurements were conducted using a TA-Q2000 DSC with a constant sweep rate of 10 K/min. Scanning electron microscopy (SEM, JEOL JSM 6500 F, Japan) coupled with energy-disperse X-ray spectroscopy (EDS) was used to characterize the microstructure and the composition of the primary and secondary phases in selected melt-spun ribbons.

3. Results and discussion

3.1. Optimization of the metal content

XRD patterns for all samples were collected at 348 K to ensure that measured lattice parameters are derived for the same magnetic state. The refinements of the XRD data revealed that all compounds crystallize in the hexagonal Fe_2P-type structure (space group *P-62 m*), as presented in Fig. 1. Upon decreasing the M/NM ratio, the amount of metal-rich impurity $(Mn,Fe)_3Si$ (space group: *Fm-3 m*) decreases. The lattice parameters derived in the PM state indicate the inflection point for the alloy y = 1.90, with a lattice parameter a = 6.01636(4) Å, and c = 3.44518(3) Å, as depicted in Fig. 2. Further reduction of the metal content contributes to the occurrence of the non-metal rich impurity $(Mn,Fe)Si$ (space group: *P2$_1$3*). The phase fractions of the two impurity phases are presented in Fig. 3, indicating a minimum total impurity content near y = 1.90. It should be noted that the minimum of two impurity phases can be found between 1.85 and 1.90. The refinements for the y = 2.00 and 1.80 samples are shown in Fig. 4. It is worth recalling that in the non-metal rich region of the $(Mn,Fe)_y(P,Si)$ family of compounds, the hexagonal $(Mn,Fe)_5Si_3$ impurity phase (space group: *P6$_3$/mcm*) is expected [6]. The unexpected formation of the $(Mn,Fe)Si$ phase is most likely related to an instability of the Fe-rich $(Mn,Fe)_5Si_3$ phase, which decomposes at temperatures below 800 °C [28,29]. This

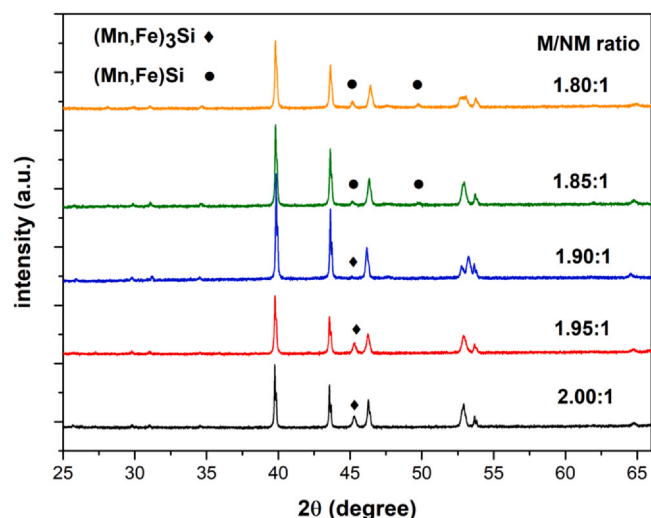**Fig. 1.** XRD patterns measured for the $(Mn,Fe)_y(P,Si)$ alloys annealed at 1373 K (y = 1.80, 1.85, 1.90, 1.95, 2.00).

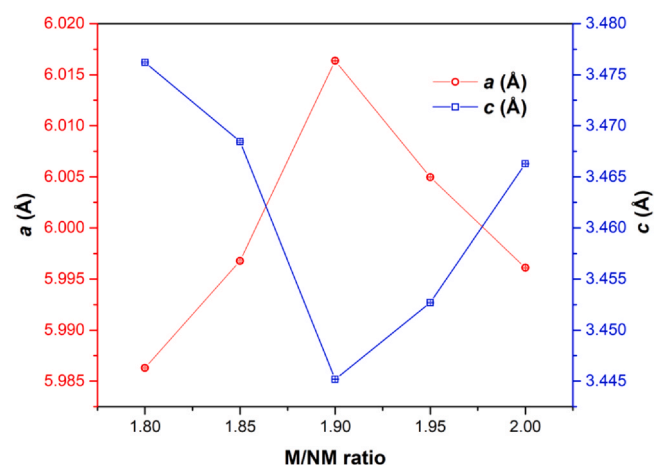**Fig. 2.** Lattice parameters a and c of the $(Mn,Fe)_y(P,Si)$ compounds, derived from the XRD patterns measured at 348 K. Error bars are within the size of the markers.
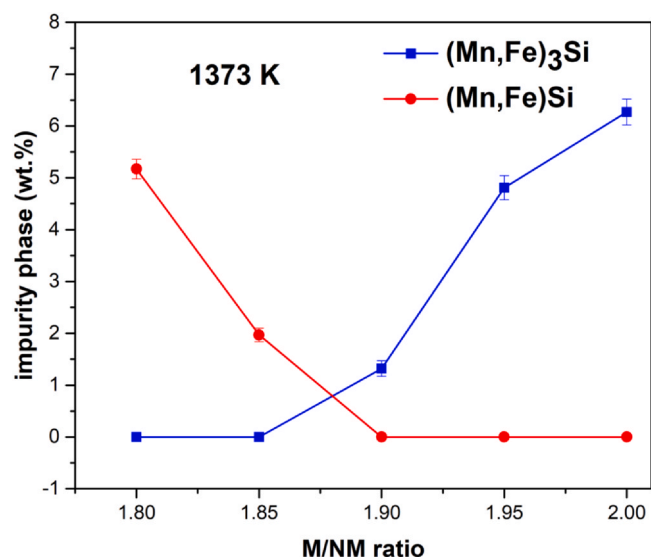

Fig. 3. Fraction of the secondary phase as a function of the M/NM ratio y.
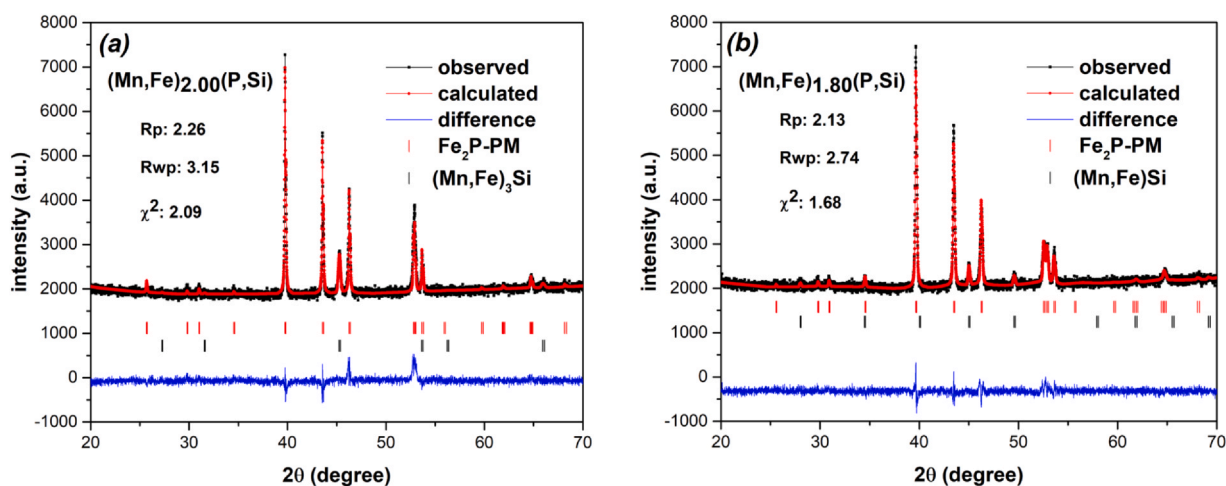
Fig. 4. Observed and calculated XRD patterns of a) $(Mn,Fe)_{2.00}(P,Si)$, b) $(Mn,Fe)_{1.80}(P,Si)$ in the paramagnetic state.

behaviour also implies an Fe-rich and Si-rich composition of this impurity phase in the investigated region of the $(Mn,Fe)_y(P,Si)$ system.

In Fig. 5 the temperature dependent magnetization (*M-T*) in an applied magnetic field of 1 T and the field dependent magnetization (*M-H*) at a temperature of 5 K are presented for the compounds annealed at 1373 K. The ferromagnetic transition temperature T_C was determined from the maximum in the temperature derivative of the magnetization $|dM/dT|$, as shown in Fig. 6a. The highest value of $|dM/dT|$ is observed for $y = 1.95$, suggesting the largest magnetic entropy change $|\Delta S_m|$. Decreasing y from 2.00 to 1.90 initially results in an increase in T_C from 251.3 to 310.1 K and a decrease in thermal hysteresis (ΔT_{hys}) from 33.3 to 8.3 K. A further decrease in the metal content y results in a decrease in T_C and a significant increase in hysteresis; by lowering y from 1.90 to 1.80 the value of T_C is reduced to 178.5 K and the thermal hysteresis is enhanced to 75.7 K. These pronounced changes in T_C and ΔT_{hys} upon decreasing the metal content might be a consequence of a significant Si depletion caused by the occurrence of the non-metal rich $(Mn,Fe)Si$ impurity phase. The values of $|\Delta S_m|$ were calculated from the isothermal magnetization curves using the Maxwell equation:

$$\Delta S_m(T,H) = \int_{\mu_0 H_1}^{\mu_0 H_2} \left(\frac{\partial M(T)}{\partial T} \right)_H d(\mu_0 H) \tag{1}$$

The values of $|\Delta S_m|$ in a magnetic field change of 2 T are as follows: 0.8, 10.9, 13.2, 17.4, 9.9 $Jkg^{-1}K^{-1}$ for $y = 1.80, 1.85, 1.90, 1.95, 2.00$, respectively (see Fig. 6b). The highest T_C and the smallest thermal hysteresis ΔT_{hys} is observed for $y = 1.90$, which is also the composition that shows the lowest amount of impurity phases. However, the largest value of $|\Delta S_m|$ is observed for $y = 1.95$, which is due to a steeper transition and an almost equally large magnetization compared to $y = 1.90$. Similar observations were recently reported by Li and co-workers [6]. The shift of the optimal y towards a lower value ($y < 2.00$) can be due to possible losses of non-metals (P, Si) occurring during the sample preparation. Previous reports show a similar trend for compounds prepared using various methods [6], [23]. Therefore, we expect that the main reason responsible for a shift of the optimal M/NM ratio is ascribed to a prompt formation of the $(Mn,Fe)_3Si$ impurity phase, which forms when $y = 1.95$. By reducing secondary phases, the composition of the main phase is close to the nominal ratio.

The $(Mn,Fe)_2(P,Si)$ compounds are known to undergo a ferromagnetic-to-paramagnetic (FM-PM) transition upon heating. The *M-H* curve for $y = 1.80$ shows a broad magnetic hysteresis accompanied by a peculiar magnetic behaviour when the magnetic field is applied for the first time. It is noticeable that in low magnetic field (< 1 T), the *M-H* curve exhibits a typical FM-like behaviour and at higher magnetic fields, a metamagnetic transition occurs, which is incomplete even at 5 T. As seen in Fig. 7, this behaviour is not observed
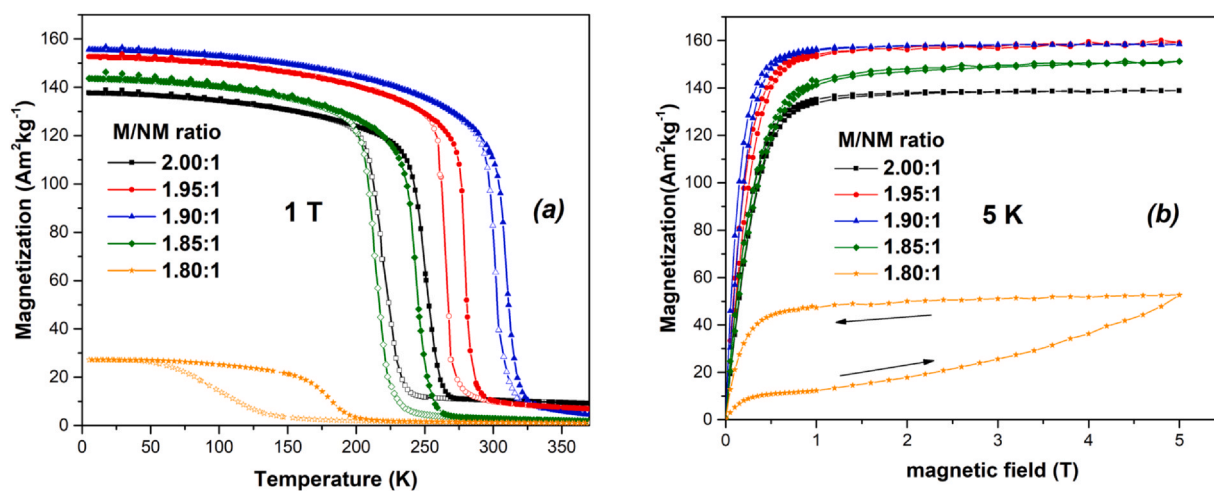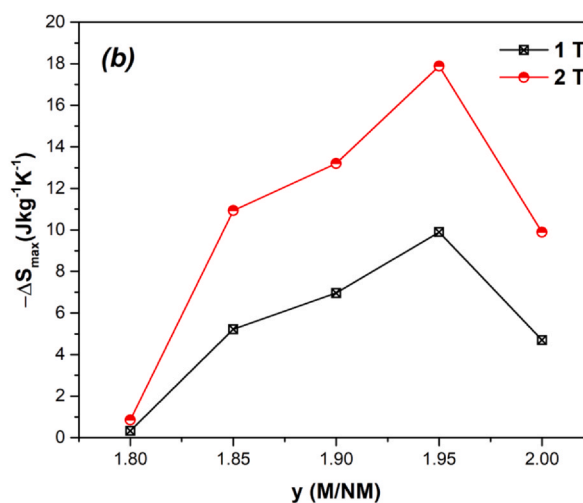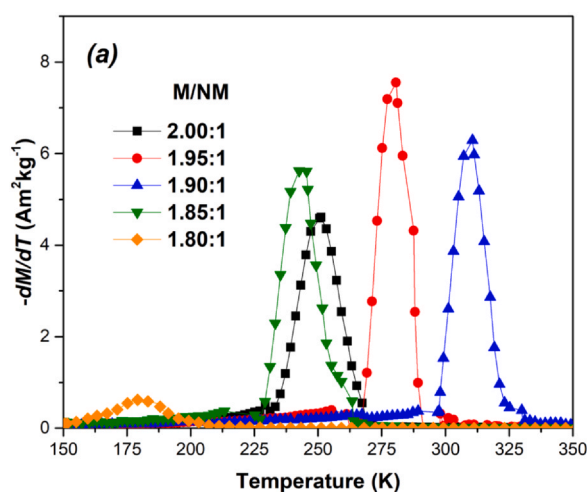

Fig. 5. a) Temperature dependent magnetization *M-T* measured in an applied field of $\mu_0 H = 1$ T and b) field dependence of magnetization *M-H* at a temperature of $T = 5$ K for the $(Mn,Fe)_y(P,Si)$ alloys annealed at 1373 K.

Fig. 6. a) Temperature derivative of the magnetization (-dM/dT) as a function of temperature measured in a field of 1 T, b) magnetic entropy change (-ΔS_m) as a function of the metal/non-metal ratio for the (Mn,Fe)$_y$(P,Si) alloys.

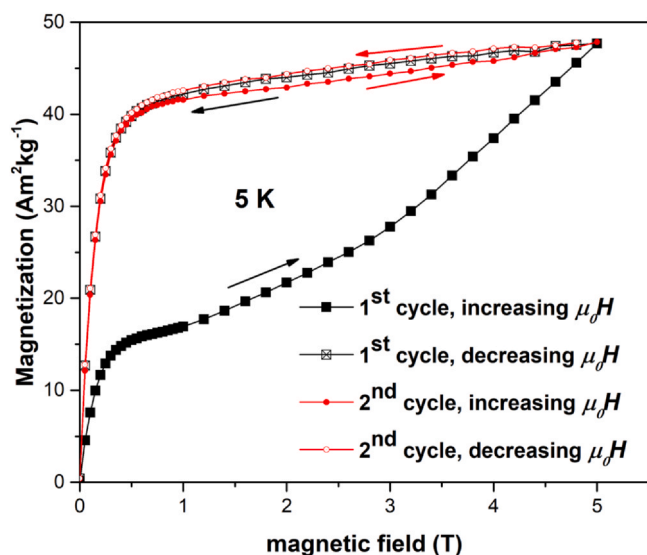**Fig. 7.** Isothermal magnetization versus magnetic field (*M-H*) curves for *y* = 1.80 measured at 5 K.
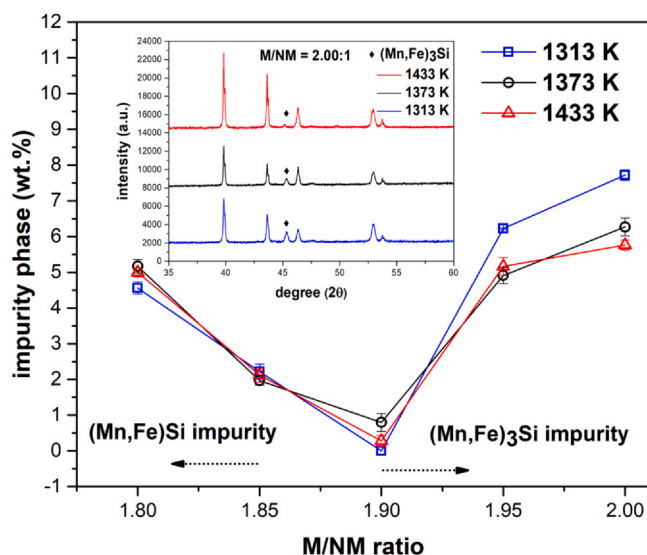

Fig. 8. Impurity phase fraction as a function of the metal/non-metal (M/NM) ratio *y* at different annealing temperatures. The inset shows the XRD patterns for *y* = 2.00 annealed at 1313, 1373 and 1433 K.

in decreasing field or in subsequent re-applied increasing magnetic field, which indicates that the initial (metastable) magnetic state is not restored. The metamagnetic transition originates from an incomplete first-order transition caused by kinetic arrest. A kinetic arrest has been reported in many materials, including the Fe$_2$P family of compounds [30–34]. The presented results show that the observed metamagnetic transition might occur as a result of the off-stoichiometry in (Mn,Fe)$_2$(P,Si) compounds.

3.2. Influence of the annealing temperature

The amount of the (Mn,Fe)$_3$Si impurity phase is slightly affected by the heat treatment conditions and shows a decreasing trend upon increasing annealing temperature, as shown in Fig. 8. As seen in the inset of Fig. 8, the diffraction peaks become sharper and narrower with increasing annealing temperature, which is attributed to enhanced homogeneity and a larger particle size. For *y* = 2.00 the amount of the (Mn,Fe)$_3$Si impurity phase fraction reduces from 7.7 to 5.5 wt.% when the annealing temperature rises from 1313 to 1433 K. The observed decrease in the (Mn,Fe)$_3$Si impurity phase shows a different trend than observed for the V-doped (Mn,Fe)$_2$(P,Si) system,

reported by Lai and co-workers [35]. For *y* = 1.80 the amount of the (Mn,Fe)Si impurity phase is hardly affected by the annealing temperature and corresponds to roughly 5 wt.%.

Fig. 9a shows that an increase in the annealing temperature from 1313 to 1373 K hardly affects the value of the *c/a* ratio. Consequently, the changes in T_C for samples annealed at 1313 and 1373 K should mainly originate from variations in the main phase composition caused by the presence of an impurity phase. The most pronounced difference appears for alloys *y* = 1.90, 1.95 and 2.00, annealed at 1433 K. As shown in Fig. 9b, the change in the *c/a* ratio is reflected by the opposite behaviour for T_C. The impact of a change in lattice parameter should be reflected most reliably by alloys containing the lowest amount of secondary phase. With increasing annealing temperature, the lattice parameter *a* increases by 0.08 % and lattice parameter *c* decreases by 0.2 % in the compound *y* = 1.90. An increase in the lattice parameter *a* leads to an increase in the distance between Fe and Si atoms in the *a-b* plane, which results in weakened chemical bonding. An opposite behaviour of the lattice parameter *c* causes a decrease in the distance between the interlayers of Mn and Fe atoms. These changes are expected to result in enhanced
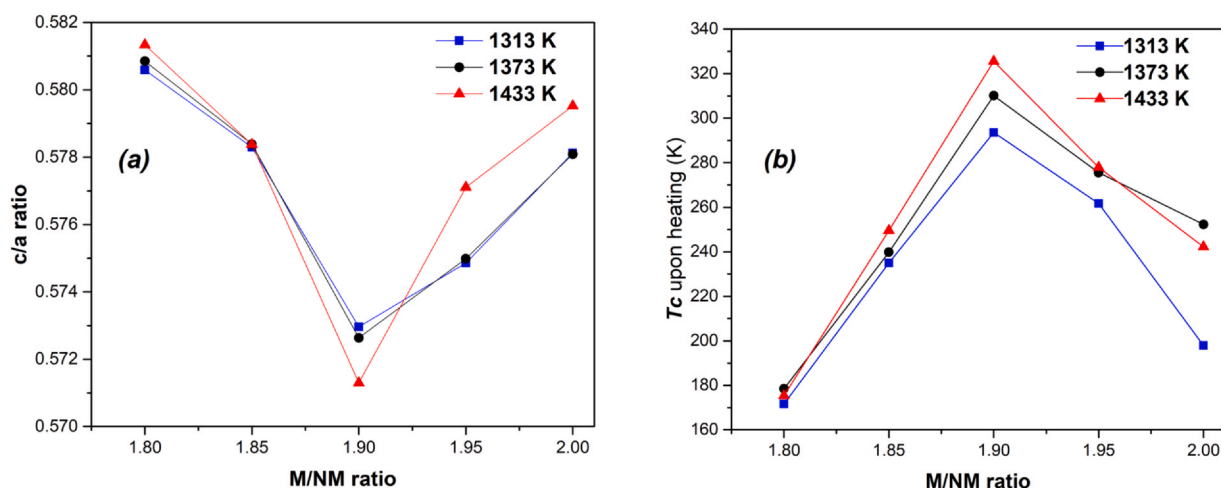
Fig. 9. Changes in a) *c/a* ratio and b) T_C as a function of the metal/non-metal (M/NM) ratio *y* for different annealing temperatures.
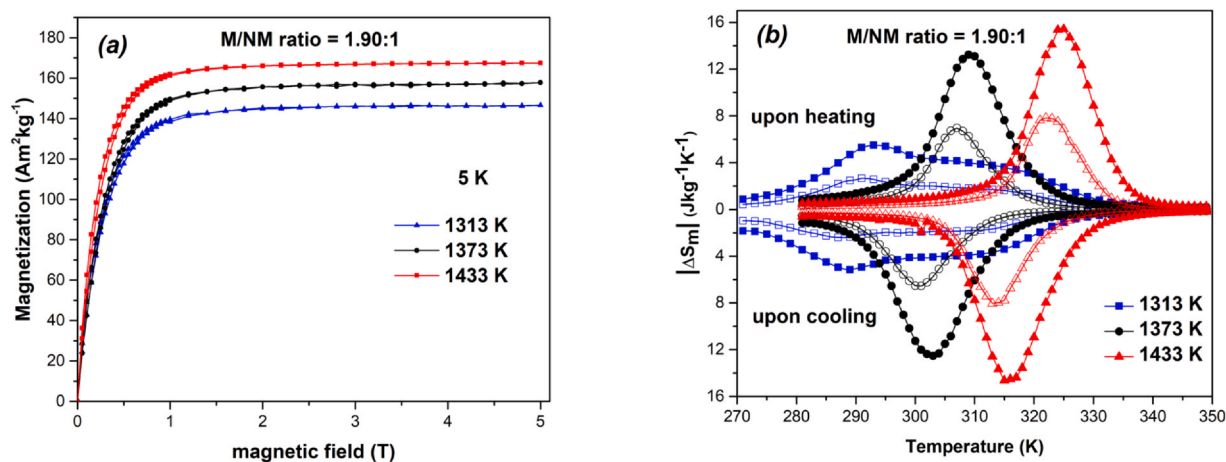

Fig. 10. Impact of the annealing temperature on a) the saturation magnetization (M_s), b) the magnetic entropy change $|\Delta S_m|$ in 1 T (open symbols) and 2 T (filled symbols) of the alloy *y* = 1.90.

Table 1

Collected data of T_C, ΔT_{hys}, *L* and M_s for (Mn,Fe)$_y$(P,Si) annealed at 1313, 1373 and 1433 K. The latent heat *L* of the sample with *y* = 1.80 was not measured because the transition temperature occurs below the calibrated range of the DSC.

y	1313 K				1373 K				1433 K			
	T_C (K)	ΔT_{hys} (K)	*L* (Jg^{-1})	M_s (Am^{2}kg^{-1})	T_C (K)	ΔT_{hys} (K)	*L* (Jg^{-1})	M_s (Am^{2}kg^{-1})	T_C (K)	ΔT_{hys} (K)	*L* (Jg^{-1})	M_s (Am^{2}kg^{-1})
1.80	171.6	71.8	–	36.1	178.5	75.7	–	52.6	175.4	79.2	–	61.3
1.85	235.0	19.0	1.9	148.4	239.8	22.1	4.8	151.2	249.6	31.6	5.3	156.8
1.90	293.6	1.9	1.1	146.6	310.1	8.3	6.5	157.8	325.6	9.9	7.4	167.5
1.95	261.7	5.8	2.9	154.8	275.5	12.1	5.7	156.7	277.9	18.3	6.6	158.7
2.00	197.9	22.1	0.4	133.7	251.3	33.3	5.1	138.8	242.2	39.9	3.8	152.8

magnetic interactions [36,37]. As a result, in Fig. 10a an increase in T_C and in saturation magnetization (M_s) is found upon an increasing annealing temperature. A sharper magnetic transition and an increase in M_s leads to an increase in $|\Delta S_m|$, as depicted in Fig. 10b. This highlights the positive impact of the highest annealing temperature but it should be noted that exceeding the temperature of 1433 K might result in melting of the alloy [7]. From Table 1 it can be observed that ΔT_{hys} and latent heat (*L*) increase simultaneously with annealing temperature in compounds containing a relatively low amount of secondary phases (*y* = 1.85–1.95), indicating an

enhancement of the FOMT for these compounds. These changes are accompanied by an increase in M_s which is caused by improved homogeneity and changes in the interatomic distances, as previously discussed. As can be seen for *y* = 1.90 in Fig. 10b, $|\Delta S_m|$ increases greatly from 5.5 to 15.5 Jkg^{-1}K^{-1}, whereas ΔT_{hys} increases from 1.9 to 9.9 K. The presence of a broad double peak in $|\Delta S_m|$ indicates that an annealing temperature of 1313 K is insufficient to provide homogeneity. In the (Mn,Fe)$_2$(P,Si) alloys, the FOMT originates from an electronic redistribution around the *3f* site. Hence, the enhancement of the FOMT upon increasing annealing temperature can be linked to

Table 2
Refined occupancies of Fe at the *3f* and *3g* site for $(Mn,Fe)_y(P,Si)$ annealed at 1313, 1373 and 1433 K. It is assumed that Mn exclusively occupies the *3g* site [38].

y	1313 K		1373 K		1433 K	
	3f (Fe)	*3g (Fe)*	*3f (Fe)*	*3g (Fe)*	*3f (Fe)*	*3g (Fe)*
1.80	0.216(1)	0.049(1)	0.221(2)	0.057(1)	0.222(1)	0.059(1)
1.85	0.182(2)	0.048(1)	0.191(3)	0.051(2)	0.193(1)	0.071(2)
1.90	0.222(1)	0.068(2)	0.236(1)	0.076(2)	0.246(2)	0.073(1)
1.95	0.180(1)	0.056(3)	0.197(1)	0.051(2)	0.268(1)	0.072(1)
2.00	0.208(2)	0.091(1)	0.256(1)	0.066(1)	0.264(1)	0.084(1)

changes in the lattice parameters and an increased Fe occupation at the *3f* site [35], as indicated by XRD refinements. The refined occupancies of Fe are summarized in Table 2. An unexpected change in latent heat can be observed for $y = 2.00$; the highest value of the latent heat is observed for the alloy annealed at 1373 K. This result indicates the strongest FOMT at the annealing temperature of 1373 K, which is most probably related to changes in the composition of the main phase.

3.3. Microstructure and impurity phase formation

To investigate the effect of the annealing temperature and metal content on the microstructure, the impurity phase formation and its influence on the magnetic properties, SEM/EDS analysis was performed for 6 samples: $y = 1.80$ and 2.00, annealed at 1313, 1373 and 1433 K.

In the $(Mn,Fe)_2(P,Si)$ system grain boundaries are preferred places for the formation of the $(Mn,Fe)_3Si$ impurity phase. Secondary phases tend to collect at grain boundaries, which lowers the interfacial energy between neighbouring crystallites [39,40]. As shown in Fig. 11a-c, the $(Mn,Fe)Si$ impurity phase segregates in the form of oval-shaped inclusions in the grain interior. The effect of the

annealing temperature on the formation of this impurity phase is found to be negligible. However, a reduction in the number of smaller inclusions ($< 1 \mu m$) is noticeable, most probably due to a coarsening into larger particles as the total amount of the impurity phase remained constant according to the XRD refinements. In addition to this, the composition of the $(Mn,Fe)Si$ phase does not significantly change for increasing annealing temperatures. Therefore, the observed increase in the Fe content for the main phase might be ascribed to an enhanced homogeneity. The Si content shows the opposite trend, which in consequence, leads to minor changes in T_C. Alternatively, the rise in Fe content might indicate the presence of an amorphous Fe-rich impurity (not visible with XRD), which decreases with increasing annealing temperature. The compositions of the primary and impurity phases are collected in Table 3. It can be noticed that the observed M/NM ratio of both the main and the impurity phase show some deviation from the expected composition. As the Mn/Fe ratio is in good agreement with the expected values, the obtained metal-rich compositions result from a deficiency of the non-metal that could possibly occur during sample preparation and/ or as a result of the impurity phase formation. The Fe-rich and Si-rich composition of the impurity phase confirms that this phase is a product of Fe_5Si_3 degradation, as indicated in Section 3.1. In the $(Mn,Fe)_2(P,Si)$ family of compounds T_C increases and the hysteresis decreases with increasing Fe and Si contents [20,41]. Therefore, the occurrence of this impurity phase might contribute to a significant decrease in T_C and an increase in hysteresis, which is observed for $y = 1.85$ and 1.80.

Contrary to the non-metal-rich region, it appeared that the annealing temperature had a notable impact on the formation and the composition of the metal-rich $(Mn,Fe)_3Si$ impurity phase. It can be seen in the inset of Fig. 12a, that after the annealing at 1313 K the compound is still inhomogeneous, as demonstrated by the presence of dendritic structures [24], which is in agreement with previously discussed magnetization results. As depicted in Fig. 12a-c, upon a
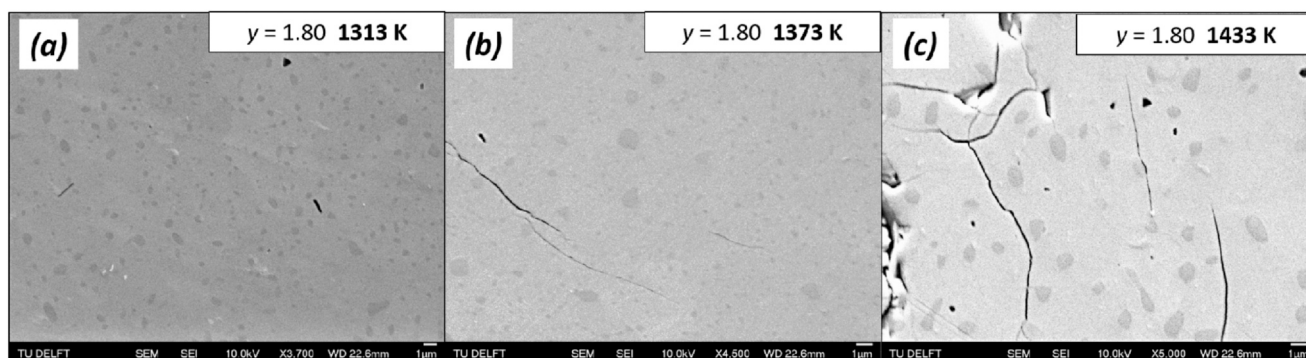

Fig. 11. SEM images of $(Mn,Fe)_{1.80}(P,Si)$ annealed at a) 1313 K, b) 1373 K, c) 1433 K.

Table 3
Compositions of the main and secondary phases in $(Mn,Fe)_{1.80}(P,Si)$ and $(Mn,Fe)_{2.00}(P,Si)$ alloys annealed at 1313, 1373 and 1433 K.

Alloy	Main phase (*at.%*)	Secondary phase (*at.%*)	M/NM ratio	
			Main phase	Secondary phase
$y = 2.00 - 1313$ K	$Mn_{26.9}Fe_{47.0}P_{19.0}Si_{7.1}$	$Mn_{15.0}Fe_{61.9}P_{4.6}Si_{18.5}$	2.83	3.33
$y = 2.00 - 1373$ K	$Mn_{25.6}Fe_{48.7}P_{18.2}Si_{7.5}$	$Mn_{14.9}Fe_{63.5}P_{0.8}Si_{20.8}$	2.89	3.63
$y = 2.00 - 1433$ K	$Mn_{26.1}Fe_{47.9}P_{18.7}Si_{7.3}$	$Mn_{12.5}Fe_{66.8}P_{0.4}Si_{20.3}$	2.84	3.83
$y = 1.80 - 1313$ K	$Mn_{27.5}Fe_{46.5}P_{19.2}Si_{7.1}$	$Mn_{6.3}Fe_{51.3}P_{1.2}Si_{41.2}$	2.81	1.36
$y = 1.80 - 1373$ K	$Mn_{26.7}Fe_{47.4}P_{19.3}Si_{6.6}$	$Mn_{6.7}Fe_{50.3}P_{2.1}Si_{40.9}$	2.86	1.33
$y = 1.80 - 1433$ K	$Mn_{26.6}Fe_{48.3}P_{18.7}Si_{6.4}$	$Mn_{6.4}Fe_{51.3}P_{1.3}Si_{41.0}$	2.98	1.36

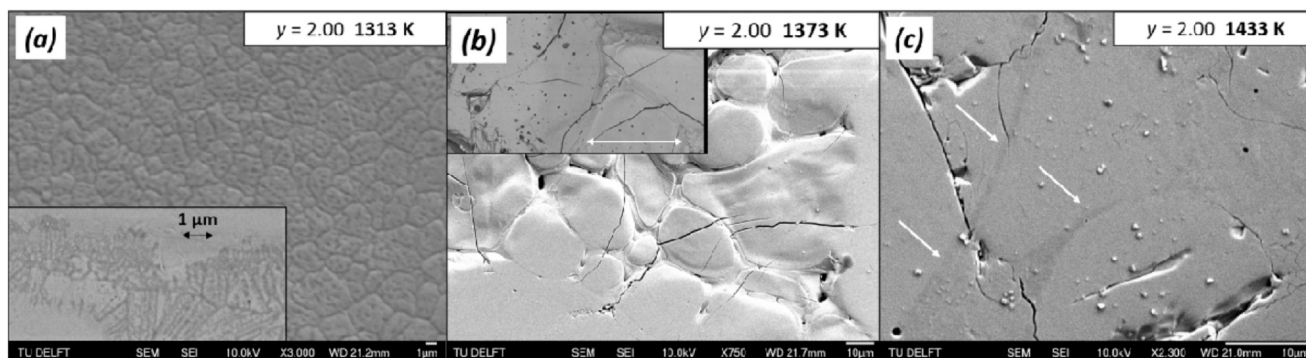Experimental uncertainties: Mn: ± 1.7 at.%, Fe: ± 1.2 at.%, P: 0.2 at.%, Si ± 0.2 at.%.

Fig. 12. SEM images of (Mn,Fe)$_{2.00}$(P,Si) annealed at a) 1313 K, b) 1373 K, c) 1433 K. The insets show BSE images of a) dendritic-like structures, b) grain boundary region. Grain boundary precipitates are indicated by arrows.

further increase in the annealing temperature, grain growth can be observed, while the dendritic structures disappear. The grain size of the $y = 2.00$ sample annealed at 1313 K does not exceed 5 μm and grain boundaries are pronounced, indicating an accumulation of the metal-rich impurity in this region. The increase in annealing temperature to 1373 K caused an enlargement of grains to about 30 μm. This grain growth is accompanied by a decrease in their number density, which also reduces the number of possible sites for the precipitation of the impurity phase. Hence, the reduction in grain-boundary density might contribute to a decreasing amount of the (Mn,Fe)$_3$Si phase, as reported in Section 3.2. After annealing at the highest temperature (1433 K), only fragmentary grain boundary precipitates are observed (indicated by arrows). Slight changes in composition of this impurity phase are observed, unlike the previously discussed (Mn,Fe)Si phase. It can be seen that with increasing annealing temperature, the amount of Fe in the impurity phase increases and the content of P decreases. Both the decrease in the amount of the secondary phase and the change in its composition directly impacts the composition of the main phase and thus, the magnetic properties. The highest T_C is observed for the alloy annealed at 1373 K, as an increase in Fe and Si content leads to a rise in T_C. Likewise, the lowest T_C is found for the alloy annealed at 1313 K as the Fe and Si content in this compound is the lowest. It is worth to recall that the difference in the c/a ratio for alloys annealed at 1313 and 1373 K is negligible. It is also worth emphasising that despite a linear decrease in the amount of the (Mn,Fe)$_3$Si phase, this trend is not observed for T_C due to changes in the composition of the secondary phase. The presented results show that optimization of the heat treatment in the (Mn,Fe)$_y$(P,Si) requires a careful consideration of the secondary phases and their transformation behaviour during the annealing process.

4. Conclusions

The effect of the annealing temperature and the optimization of the metal/non-metal ratio was investigated in Fe-rich (Mn,Fe)$_y$(P,Si) melt-spun ribbons. While y decreases from 2.00 to 1.90, a reduction in the metal-rich impurity phase (Mn,Fe)$_3$Si, an increase in the Curie temperature (T_C) and a decrease in thermal hysteresis (ΔT_{hys}) is observed. A further decrease of metal content from 1.90 to 1.80 caused a decrease in T_C and a significant increase in ΔT_{hys}. Additionally, in the metal-deficient region of (Mn,Fe)$_y$(P,Si), the formation of the (Mn,Fe)Si phase is observed, which is assigned to a

degradation of the unstable and primary formed Fe$_5$Si$_3$ compound. With increasing annealing temperature, an increase in $|\Delta S_{ml}|$, T_C and ΔT_{hys} is observed in the optimized compound ($y = 1.90$), indicating an enhancement of the FOMT. It was found that the annealing temperature hardly influences the formation and the composition of the (Mn,Fe)Si impurity phase. On the other hand, the amount of the (Mn,Fe)$_3$Si impurity phase slightly decreased with increasing annealing temperature, which might be assigned to grain growth and a reduced number of grain boundaries. A decrease in the (Mn,Fe)$_3$Si impurity phase content was accompanied by changes in the main phase composition, which was directly reflected in the magnetic properties of the prepared compounds.

CRediT authorship contribution statement

Anika Kiecana: Conceptualization, Methodology, Investigation, Writing – original draft. **Cees Kwakernaak**: Investigation, Formal analysis. **Niels van Dijk:** Conceptualization, Supervision, Writing – review & editing, Funding acquisition. **Ekkes Brück:** Conceptualization, Supervision, Writing – review & editing, Funding acquisition.

Data Availability

Data will be made available on request.

Declaration of Competing Interest

The authors declare that they have no known competing financial interests or personal relationships that could have appeared to influence the work reported in this paper.

References

[1] P. Weiss, A. Piccard, Le phénomène magnétocalorique, J. Phys. Theor. Appl. vol. 7, (1) (1917) 103–109.

[2] M.P. Annaorazov, et al., Alloys of the FeRh system as a new class of working material for magnetic refrigerators, Cryogenics vol. 32, (10) (1992) 867–872, https://doi.org/10.1016/0011-2275(92)90352-B

[3] V.K. Pecharsky, K.A. Gschneidner, Giant magnetocaloric effect in $Gd_5(Si_2Ge_2)$, Phys. Rev. Lett. vol. 78, (23) (1997) 4494–4497, https://doi.org/10.1103/PhysRevLett.78.4494

[4] C. Zimm, et al., Description and Performance of a Near-Room Temperature Magnetic Refrigerator, in: P. Kittel (Ed.), Advances in cryogenic engineering, Springer US, Boston, MA, 1998, pp. 1759–1766.

[5] E. Brück, Developments in magnetocaloric refrigeration, J. Phys. D. Appl. Phys. vol. 38, (23) (2005) 381–391, https://doi.org/10.1088/0022-3727/38/23/R01

[6] C.F. Li, et al., Effect of M/NM ratios on structural and magnetic properties of $(Mn,Fe)_2(P,Si)$ compounds, Phys. B Condens. Matter vol. 594, (2020), https://doi.org/10.1016/j.physb.2020.412309

[7] Z.G. Zheng, et al., Large magnetic entropy change and magnetic phase transitions in rapidly quenched bulk Mn-Fe-P-Si alloys, J. Alloy. Compd. vol. 725, (2017) 1069–1076, https://doi.org/10.1016/j.jallcom.2017.07.243

[8] Z.Q. Ou, et al., Transition metal substitution in Fe_2P-based $MnFe_{0.95}P_{0.50}Si_{0.50}$ magnetocaloric compounds, J. Alloy. Compd. vol. 730, (2018) 392–398, https://doi.org/10.1016/j.jallcom.2017.09.315

[9] R.R. Gimaev, et al., Peculiarities of magnetic and magnetocaloric properties of fe-rh alloys in the range of antiferromagnet–ferromagnet transition, Phys. Met. Metallogr. vol. 121, (9) (2020) 823–850, https://doi.org/10.1134/S0031918×20090045

[10] Y. Cao, et al., Phase transition and magnetocaloric effect in particulate Fe-Rh alloys, J. Mater. Sci. vol. 55, (27) (2020) 13363–13371, https://doi.org/10.1007/s10853-020-04921-y

[11] A. Chirkova, et al., Giant adiabatic temperature change in FeRh alloys evidenced by direct measurements under cyclic conditions, Acta Mater. vol. 106, (2016) 15–21, https://doi.org/10.1016/j.actamat.2015.11.054

[12] A. Magnus, et al., The magnetic and magnetocaloric properties of $Gd_5Ge_2Si_2$ compound under hydrostatic pressure, J. Appl. Phys. vol. 97, (10) (2005) 2003–2006, https://doi.org/10.1063/1.1860932

[13] C.S. Alves, et al., Giant magnetocaloric effect in $Gd_5(Si_2Ge_2)$ alloy with low purity Gd, Mater. Res. vol. 7, (4) (2004) 535–538, https://doi.org/10.1590/s1516-14392004000400005

[14] J. Lyubina, et al., Novel design of $La(Fe,Si)_{13}$ alloys towards high magnetic refrigeration performance, Adv. Mater. vol. 22, (2010) 3735–3739, https://doi.org/10.1002/adma.201000177

[15] V. Paul-Boncour, L. Bessais, Tuning the magnetocaloric properties of the La $(Fe,Si)_{13}$ compounds by chemical substitution and light element insertion, Magnetochemistry vol. 7, (1) (2021) 1–18, https://doi.org/10.3390/magnetochemistry7010013

[16] A. Boutahar, et al., Theoretical work in magnetocaloric effect of $LaFe_{13-x}Si_x$ compounds, J. Supercond. Nov. Magn. vol. 27, (8) (2014) 1795–1800, https://doi.org/10.1007/s10948-014-2542-z

[17] A. Yan, et al., Magnetic entropy change in melt-spun MnFePGe (invited, J. Appl. Phys. vol. 99, (8) (2006), https://doi.org/10.1063/1.2162807

[18] Z.Q. Ou, et al., Interstitial boron in MnFe(P,As) giant-magnetocaloric alloy, Results Phys. vol. 2, (2012) 110–113, https://doi.org/10.1016/j.rinp.2012.09.005

[19] M. Yue, et al., Crystal structure and magnetic transition of MnFePGe compound prepared by spark plasma sintering, J. Appl. Phys. vol. 105, (7) (2009) 7–10, https://doi.org/10.1063/1.3056157

[20] Z.Q. Ou, et al., Structure, magnetism and magnetocalorics of Fe-rich $(Mn,Fe)_{1.95}P_{1-x}Si_x$ melt-spun ribbons, J. Alloy. Compd. vol. 710, (2017) 446–451, https://doi.org/10.1016/j.jallcom.2017.03.266

[21] P. Devi, et al., Improved magnetostructural and magnetocaloric reversibility in magnetic Ni-Mn-In shape-memory Heusler alloy by optimizing the geometric compatibility condition, Phys. Rev. Mater. vol. 3, (6) (2019) 1–6, https://doi.org/10.1103/PhysRevMaterials.3.062401

[22] A.M. Aliev, et al., Magnetocaloric effect in ribbon samples of Heusler alloys Ni-Mn-M (M = In,Sn), Appl. Phys. Lett. vol. 97, (21) (2010), https://doi.org/10.1063/1.3521261

[23] M. Fries, et al., Microstructural and magnetic properties of Mn-Fe-P-Si (Fe_2P-type) magnetocaloric compounds, Acta Mater. vol. 132, (2017) 222–229, https://doi.org/10.1016/j.actamat.2017.04.040

[24] J.W. Lai, et al., Microstructure formation and magnetocaloric effect of the Fe_2P-type phase in $(Mn,Fe)_2(P, Si, B)$ alloys, J. Alloy. Compd. vol. 735, (2018) 2567–2573, https://doi.org/10.1016/j.jallcom.2017.11.287

[25] J. Lai, et al., Tuning the magneto-elastic transition of $(Mn,Fe,V)_2(P,Si)$ alloys to low magnetic field applications, J. Alloy. Compd. vol. 821, (2020) 153451, https://doi.org/10.1016/j.jallcom.2019.153451

[26] N.V. Thang, et al., Effect of heat treatment conditions on MnFe(P,Si,B) compounds for room-temperature magnetic refrigeration, J. Alloy. Compd. vol. 699, (2017) 633–637, https://doi.org/10.1016/j.jallcom.2016.12.402

[27] H.M. Rietveld, A profile refinement method for nuclear and magnetic structures, J. Appl. Crystallogr. vol. 2, (2) (1969) 65–71, https://doi.org/10.1107/s0021889869006558

[28] D.B. Rogers, Magnetic and mössbauer effect studies of Mn5Si3: Fe5Si3 solid solutions, J. Solid State Chem. vol. 323, (1972) 311–323.

[29] L. Pal, et al., Effect of Mn substitution on the magnetic and magneto-transport properties of $Fe_{3-x}Mn_xSi$ ($0 \leq x \leq 1.25$) alloys, J. Appl. Phys. vol. 113, (9) (2013) 0–7, https://doi.org/10.1063/1.4794126

[30] X.F. Miao, et al., "Kinetic-arrest-induced phase coexistence and metastability in $(Mn,Fe)_2(P,Si)$", Phys. Rev. B vol. 94, (9) (2016), https://doi.org/10.1103/PhysRevB.94.094426

[31] V.K. Sharma, et al., Kinetic arrest of the first order austenite to martensite phase transition in $Ni_{50}Mn_{34}In_{16}$: Dc magnetization studies, Phys. Rev. B - Condens. Matter Mater. Phys. vol. 76, (14) (2007) 3–6, https://doi.org/10.1103/PhysRevB.76.140401

[32] A. Banerjee, et al., Conversion of a glassy antiferromagnetic-insulating phase to an equilibrium ferromagnetic-metallic phase by devitrification and re-crystallization in Al substituted $Pr_{0.5}Ca_{0.5}MnO_3$, J. Phys. Condens. Matter vol. 21, (2) (2009) 0–12, https://doi.org/10.1088/0953-8984/21/2/026002

[33] A. Banerjee, et al., Coexisting tunable fractions of glassy and equilibrium long-range-order phases in manganites, J. Phys. Condens. Matter vol. 18, (49) (2006) 1–9, https://doi.org/10.1088/0953-8984/18/49/L02

[34] X.F. Miao, et al., Tuning the magnetoelastic transition in $(Mn,Fe)_2(P,Si)$ by B, C, and N doping, Scr. Mater. vol. 124, (2016) 129–132, https://doi.org/10.1016/j.scriptamat.2016.07.015

[35] J. Lai, et al., Combined effect of annealing temperature and vanadium substitution for magnetocaloric $Mn_{1.2-x}V_xFe_{0.75}P_{0.5}Si_{0.5}$ alloys, J. Alloy. Compd. vol. 803, (2019) 671–677, https://doi.org/10.1016/j.jallcom.2019.06.239

[36] E.K. Delczeg-Czirjak, et al., Magnetic exchange interactions in B-, Si-, and As-doped Fe_2P from first-principles theory, Phys. Rev. B - Condens. Matter Mater. Phys. vol. 85, (22) (2012) 1–7, https://doi.org/10.1103/PhysRevB.85.224435

[37] I. Batashev, et al., Lithiation of the Fe_2P-based magnetocaloric materials: A first-principles study, J. Magn. Magn. Mater. 537, (2021) 168179, https://doi.org/10.1016/j.jmmm.2021.168179

[38] Z.Q. Ou, et al., Neutron diffraction study on the magnetic structure of Fe_2P-based $Mn_{0.66}Fe_{1.29}P_{1-x}Si_x$ melt-spun ribbons, J. Magn. Magn. Mater. vol. 340, (2013) 80–85, https://doi.org/10.1016/j.jmmm.2013.03.028

[39] C. Vargel, Intergranular corrosion, Corros. Alum. (2020) 185–197, https://doi.org/10.1016/b978-0-08-099925-8.00015-6

[40] G. Gottstein, L.S. Shvindlerman, Grain Boundary Migration in Metals: Thermodynamics, Kinetics, Application, CRC Press, 1999.

[41] J.V. Leitão, et al., Magnetic and magnetocaloric exploration of Fe rich $(Mn,Fe)_2(P,Ge)$, J. Magn. Magn. Mater. vol. 344, (2013) 49–54, https://doi.org/10.1016/j.jmmm.2013.05.032